Modeling collagen recruitment in hyperelastic bio-material models with statistical distribution of the fiber orientation

Alessio Gizzi [a,*], Marcello Vasta [b], Anna Pandolfi [c]

[a] University Campus Bio-Medico of Rome, Engineering Faculty, via A. del Portillo 21, 00128 Rome, Italy
[b] Università di Chieti-Pescara, Dipartimento INGEO, Viale Pindaro 42, Pescara, Italy
[c] Politecnico di Milano, Dipartimento di Ingegneria Civile ed Ambientale, Piazza Leonardo da Vinci 32, Milano, Italy

Article history:
Received 26 December 2013
Received in revised form 28 January 2014
Accepted 8 February 2014

1. Introduction

Fiber reinforced bio-materials show strongly nonlinear and anisotropic responses (Destrade et al., 2009; Merodio and Ogden, 2005). Many biological tissues, in particular, are characterized by a functional micro-architecture of collagen fibers and are modeled conveniently as an underlying isotropic matrix embedded with one or more sets of fibers (Fereidoonnezhad et al., 2013). At small strains the dominant response is provided by the isotropic component, while for larger strains the collagen fibers, initially crimped, gradually unfurl and begin bearing some loading (Roach and Burton, 1957). The contribution of the uncrimped fibers becomes dominant for large strains.

Most of material models commonly used in applications assume that the contribution of fibers, although marginally, manifests even at low strains (Gasser et al., 2006; Holzapfel et al., 2000; Pandolfi and Vasta, 2012). There are experimental examples, though, of activation of the fibers at a particular, finite, strain threshold. Abrupt fiber recruitment has been considered in material modeling (Li and Robertson, 2009; Watton et al., 2012; Wulandana and Robertson, 2005), but the direct measurement of the process has been posing challenges to experimentalists. Recent studies proposed to use multi-photon microscopy (MPM) combined with biomechanical devices to visualize the collagen structure in segments of biological tissue

* Corresponding author. Tel.: +39 06225419660.
E-mail addresses: a.gizzi@unicampus.it (A. Gizzi), mvasta@unich.it (M. Vasta), anna.pandolfi@polimi.it (A. Pandolfi).

at different strains (Megens et al., 2007; Zoumi et al., 2004). An accurate experimental program on carotid arteries where non destructive uniaxial tests joined with MPM provided a good collection of stretched collagen fiber and elastin images has been recently discussed in Hill et al. (2012).

As far as the theoretical aspects are concerned, several years ago Lanir (1979, 1983) formulated a three-dimensional structural model of planar collagenous tissues—e.g. skin—accounting for the distribution of collagen fiber orientation and for fiber recruitment. Subsequently, Sacks (2000) incorporated directly in Lanir's model the distribution of the fiber orientation obtained from small angle light scattering, and characterized the recruitment probability distribution function (PDF) with parameters obtained from a least-squares fit of experimental data. More recently collagen fiber recruitment defined by a PDF, but assumed to initiate at an infinitesimal strain, has been quantified in rabbit carotid arteries using staining and fixation with confocal microscopy (Roy et al., 2010).

On the basis of their own experimental results, to describe gradual recruitment at finite strains Hill et al. (2012) proposed an alternative form of the strain energy function, characterized by stretches defined on a PDF. The mechanical parameters feeding the material model were identified directly from experimental measurements.

Some biological tissues show a relatively thin two-dimensional structure, resulting from the particular interlacing architecture of reinforcing collagen fibers. Recently, the mathematical characterization of such tissues has seen important advances (Soldatos, 2009). Among others, we can mention the spatial distribution of the fiber orientation (Alastrué et al., 2006; Federico and Gasser, 2010; Gasser et al., 2006; Kroon and Holzapfel, 2008; Pandolfi and Vasta, 2012; Pinsky et al., 2005; Raghupathy and Barocas, 2009; Roy et al., 2010; Vasta et al., 2013; Wang et al., 2012).

In the present contribution we consider a class of material models characterized by a spatial distribution of the orientation of the fibers, adopting an approximated formulation of the strain energy density. We start from the Taylor expansion of the strain energy about the average fourth invariant $\bar{I}_4^*$ of the distribution (Pandolfi and Vasta, 2012), truncated at the quadratic terms. Then, the stochastic material model, referred to as *second order, or variance, approximation*, is enriched with a collagen recruitment mechanism (Hill et al., 2012), described with a recruitment function likewise expanded about $\bar{I}_4^*$ up to the quadratic terms. We derive the explicit expressions of the stress and elasticity tensors of the proposed material model. The new stochastic model is compared with previous material models and validated against experimental results.

We show that the highly nonlinear behavior of the recruitment model is well described by the proposed second order formulation of a strain energy with a von Mises distribution of the fiber orientation. Numerical simulations of uniaxial tests show that the approximation provided by the second order or variance approach is more accurate than the approximation based on the first order, or mean, formulation. Upon experimental data set tuning, the present theoretical formulation allows for the parametric characterization of the mean and variance contributions to the average stress and tangent stiffness tensors.

It is important to emphasize that the present approach is slightly different from others currently discussed in the literature. In particular, we note that the expression *second order* used here to denote the approximation of a statistical distribution of fibers should not be confused with the second order terms of the Landau and Lifshitz expansion of isotropic strain energy densities (Landau and Lifshitz, 1986) described, e. g., in Destrade et al. (2010). Additionally, we remark that the fiber families here considered are characterized by a distribution of the spatial—or planar—orientation and they do not fall in the class of transversally isotropic materials, except for the case of fully aligned fibers. However, for the latter case, it is not worth to use the present model. According to Spencer, transversally isotropic hyperelastic fiber reinforced materials must be described in terms of the Cauchy strain invariants $\bar{I}_1$ and $\bar{I}_2$ and of two pseudo invariants $\bar{I}_4$ and $\bar{I}_5$ that include the orientation of the fiber. Recently, it has been pointed out that the description of fiber reinforced transversally isotropic materials cannot be done in terms of only a pair of strain invariants (e. g., $\bar{I}_1$ and $\bar{I}_4$). In fact, this assumption introduces a kinematic constraint between the stretch components that cannot be satisfied in simple tension tests (Destrade et al., 2013; Murphy, 2013; Pucci and Saccomandi, 2014). Our approach, though, does not face this issue, since the description of the isotropic part of the hyperelastic strain energy is done in terms of a Mooney–Rivlin model, which depends on both $\bar{I}_1$ and $\bar{I}_2$, while the anisotropic part accounts for a distributed, not aligned, set of fibers that is described by means of average and variance measures.

The outline of the paper is as follows. In Section 2 we introduce the general hyperelastic formulation and the statistical distribution of fibers in terms of both first and second order approximations. In Section 3 we specialize the general three-dimensional formulation to a planar fiber distribution. In Section 4 we introduce material models able to describe the fiber recruitment process. The numerical response and parameter tuning upon experimental uniaxial tests are reported in Section 5, whereas conclusions and future perspectives are drawn in Section 6.

2. Fully three-dimensional fiber orientation distribution

We are concerned with a fully hyperelastic approach, and introduce a strain energy function that describes the reversible behavior of a fibrous material characterized by reinforcing fibers embedded in an isotropic matrix. We make the assumption that the strain energy density splits into the sum of volumetric, matrix, and fiber contributions in the standard form:

$$\Psi(\mathbf{C},\mathbf{a}) = \Psi_{\text{volumetric}}(J) + \Psi_{\text{matrix}}(\overline{\mathbf{C}}) + \Psi_{\text{fiber}}(\overline{\mathbf{C}},\mathbf{a}),$$

where $\overline{\mathbf{C}} = J^{-2/3}\mathbf{C}$ is the isochoric part of the Cauchy–Green deformation tensor $\mathbf{C} = \mathbf{F}^T\mathbf{F}$, $\mathbf{F}$ the deformation gradient, $J = \det(\mathbf{F})$ the volumetric deformation, and $\mathbf{a}$ a unit vector describing the orientation of the fiber distribution in the stress free state. The expressions of $\Psi_{\text{volumetric}}(J)$ and $\Psi_{\text{matrix}}(\overline{\mathbf{C}})$ will be specified later in the application section, since we are

focusing in the anisotropic contribution due to the fibers. Within the unit sphere ω, the generic unit vector $\mathbf{a}$ is defined in terms of the two Eulerian angles $\Theta \in [0, \pi]$ and $\Phi \in [0, 2\pi]$ as

$$\mathbf{a}(\Theta, \Phi) = \sin\Theta\cos\Phi\,\mathbf{e}_1 + \sin\Theta\sin\Phi\,\mathbf{e}_2 + \cos\Theta\,\mathbf{e}_3,$$

see Fig. 1(left). It follows that also the directional structure tensor $\mathbf{A} = \mathbf{a} \otimes \mathbf{a}$ is defined in terms of Eulerian angles.

In a material with statistical distribution of the fibers, the spatial orientation of the fibers is described by a density function $\bar{\rho}$ of the unit vector $\mathbf{a}$. We assume the symmetry property $\bar{\rho}(\mathbf{a}) \equiv \bar{\rho}(-\mathbf{a})$ and the normalization property

$$\int_\omega \bar{\rho}(\mathbf{a}) d\omega = \int_0^{\pi} \int_0^{2\pi} \bar{\rho}(\mathbf{a}) \sin\Theta d\Phi d\Theta = 4\pi, \tag{1}$$

where the expression $\bar{\rho}(\mathbf{a}) \sin\Theta\, d\Theta\, d\Phi$ represents the amount of fibers whose orientation falls in the range $[(\Theta, \Theta + d\Theta), (\Phi, \Phi + d\Phi)]$. For an assigned distribution $\bar{\rho}(\mathbf{a})$ of the fiber orientation, the operator $\langle f \rangle$ returns the average over the unit sphere of the function $f(\mathbf{a})$:

$$\langle f \rangle = \frac{1}{4\pi} \int_\omega \bar{\rho}(\mathbf{a}) f(\mathbf{a})\, d\omega. \tag{2}$$

The strain energy density $\Psi_{\text{fiber}}(\overline{\mathbf{C}}, \mathbf{a})$ of a small portion of fibers oriented in the direction $\mathbf{a}$ can take different functional forms. Explicit expressions of the stress and stiffness tensors can be obtained only if the analytical form of $\Psi_{\text{fiber}}(\overline{\mathbf{C}}, \mathbf{a})$ is specified. In the following we consider a classic exponential expression often used in the literature (Gasser et al., 2006; Pandolfi and Vasta, 2012):

$$\Psi_{\text{fiber}}(\overline{\mathbf{C}}, \mathbf{a}) = \Psi_{\text{fiber}}(\bar{I}_4) = \overline{\Psi}_{\text{fiber}} + \Psi^0_{\text{fiber}} = \frac{k_1}{2k_2} \exp\left[k_2(\bar{I}_4 - 1)^2\right] - \frac{k_1}{2k_2}, \tag{3}$$

where $\bar{I}_4 = \mathbf{A} : \overline{\mathbf{C}}$ is the directional fourth pseudo-invariant of $\overline{\mathbf{C}}$. The expression (3) holds only for fibers in tension, i. e., for $\bar{I}_4 > 1$. For later perusal, we recall the derivatives:

$$\frac{\partial \overline{\Psi}_{\text{fiber}}}{\partial \bar{I}_4} = 2k_2(\bar{I}_4 - 1)\overline{\Psi}_{\text{fiber}} = M(\bar{I}_4)\overline{\Psi}_{\text{fiber}} = \mathcal{M}(\bar{I}_4), \tag{4}$$

$$\frac{\partial^2 \overline{\Psi}_{\text{fiber}}}{\partial \bar{I}_4 \partial \bar{I}_4} = 2k_2\left[2k_2(\bar{I}_4 - 1)^2 + 1\right]\overline{\Psi}_{\text{fiber}} = 2K(\bar{I}_4)\overline{\Psi}_{\text{fiber}} = \mathcal{K}(\bar{I}_4). \tag{5}$$

The second Piola–Kirchhoff stress tensor for the small portion of fibers $\overline{\mathbf{S}}_{\text{fiber}}(\bar{I}_4)$ follows as

$$\overline{\mathbf{S}}_{\text{fiber}}(\bar{I}_4) = 2\frac{\partial \Psi_{\text{fiber}}(\bar{I}_4)}{\partial \overline{\mathbf{C}}} = 2\mathcal{M}(\bar{I}_4)\mathbf{A}, \tag{6}$$

and the isochoric material stiffness tangent for the small portion of fibers $\overline{\mathbb{C}}_{\text{fiber}}(\bar{I}_4)$ follows as

$$\overline{\mathbb{C}}_{\text{fiber}}(\bar{I}_4) = 4J^{-4/3}\frac{\partial^2 \Psi_{\text{fiber}}(\bar{I}_4)}{\partial \overline{\mathbf{C}} \partial \overline{\mathbf{C}}} = 4J^{-4/3}\mathcal{K}(\bar{I}_4)\mathbf{A} \otimes \mathbf{A}.$$

For the full expression of the second Piola–Kirchhoff stress tensor and tangent stiffness tensor see, e.g., Gasser et al. (2006) and Pandolfi and Vasta (2012)). Since the isochoric deformation tensor $\overline{\mathbf{C}}$ is independent of the Eulerian angles, the average pseudo-invariant $\bar{I}_4^*$ can be computed straightforwardly as

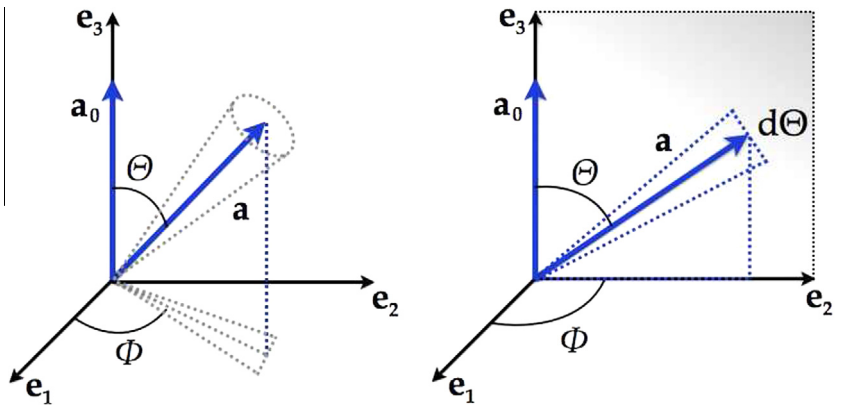

Fig. 1. Orientation of the generic unit vector aligned with a set of fibers in spherical (left) and cylindrical (right) coordinates for a planar distribution in the $(\mathbf{e}_2, \mathbf{e}_3)$ plane with $\Phi = \pi/2$.

$$\bar{I}_4^* = \langle \bar{I}_4 \rangle = \frac{1}{4\pi}\int_\omega \bar{\rho}(\mathbf{a})\bar{I}_4(\mathbf{a})\,d\omega = \frac{1}{4\pi}\int_\omega \bar{\rho}(\mathbf{a})\mathbf{A}\,d\omega : \overline{\mathbf{C}} = \mathbf{H} : \overline{\mathbf{C}}, \tag{7}$$

where $\mathbf{H} = \langle \mathbf{A} \rangle$ is a second order generalized structure tensor (GST). As first observed in Cortes et al. (2010), in the definition of $\bar{I}_4^*$ the eventual portion of fibers under compression cannot be excluded. Therefore, if one of the eigenvalues of $\overline{\mathbf{C}}$ is inferior to the unit, a fraction of compressed fibers will be included in the average of the invariant. Accordingly, the average strain energy density over the unit sphere is defined as

$$\Psi_{\text{fiber}}^* = \langle \Psi_{\text{fiber}} \rangle = \frac{1}{4\pi}\int_\omega \bar{\rho}(\mathbf{a})\Psi_{\text{fiber}}(\bar{I}_4)d\omega. \tag{8}$$

In general, for different expressions of the strain energy $\Psi_{\text{fiber}}(\overline{\mathbf{C}}, \mathbf{a})$, no close forms of (8) are available, and the hyperelastic approach loses his computational appeal since the stress tensor $\overline{\mathbf{S}}_{\text{fiber}}^*$ cannot be derived analytically, but only through the average definition

$$\overline{\mathbf{S}}_{\text{fiber}}^* = \langle \overline{\mathbf{S}}_{\text{fiber}} \rangle = \frac{1}{4\pi}\int_\omega \bar{\rho}(\mathbf{a})\overline{\mathbf{S}}_{\text{fiber}}(\bar{I}_4)d\omega. \tag{9}$$

Also the tangent stiffness $\overline{\mathbb{C}}_{\text{fiber}}^*$ can be only computed numerically as

$$\overline{\mathbb{C}}_{\text{fiber}}^* = \langle \overline{\mathbb{C}}_{\text{fiber}} \rangle = \frac{1}{4\pi}\int_\omega \bar{\rho}(\mathbf{a})\overline{\mathbb{C}}_{\text{fiber}}(\bar{I}_4)d\omega. \tag{10}$$

To alleviate the difficulties related to the evaluation of the expressions (8) and (9), alternative, simplified forms of the strain energy density have been proposed. An example is given by transversally isotropic distributions (Gasser et al., 2006) derived from the assumption of rotational symmetry of the fiber orientation distribution about a specific referential direction $\mathbf{a}_0$. Indeed this situation is important in biomechanical applications where transversally isotropy is observed (Ni Annaidh et al., 2012). In particular, the approach described in Gasser et al. (2006) leads to the definition of an approximated strain energy density $\Psi_{\text{fiber}}^{\text{GST}}$ defined in terms of the tensor $\mathbf{H}$ above introduced. As discussed in Pandolfi and Vasta (2012), the GST model can be interpreted as a linearization of the strain energy density $\Psi_{\text{fiber}}(\bar{I}_4)$ about the average invariant $\bar{I}_4^*$:

$$\Psi_{\text{fiber}}^{\text{GST}} \approx \Psi_{\text{fiber}}(\bar{I}_4^*) + \left.\frac{\partial \Psi_{\text{fiber}}}{\partial \bar{I}_4}\right|_{\bar{I}_4=\bar{I}_4^*} \langle \bar{I}_4 - \bar{I}_4^* \rangle = \overline{\Psi}_{\text{fiber}}^* + \Psi_{\text{fiber}}^0, \tag{11}$$

since, by definition of average, $\langle \bar{I}_4 - \bar{I}_4^* \rangle = 0$. The approximation (11) allows for the analytical calculation of the average stress tensor in the straightforward form as

$$\overline{\mathbf{S}}_{\text{fiber}}^{\text{GST}} = 2\mathcal{M}(\bar{I}_4^*)\mathbf{H}, \tag{12}$$

and of the average tangent stiffness tensor as

$$\overline{\mathbb{C}}_{\text{fiber}}^{\text{GST}} = 4J^{-4/3}\mathcal{K}(\bar{I}_4^*)\mathbf{H} \otimes \mathbf{H}. \tag{13}$$

Regrettably, for very dispersed fiber distributions the approximation (12), (13) is affected by large errors (Cortes et al., 2010). A better approximation is obtained by accounting for the second order terms (or variance, V) of the Taylor expansion of Ψ_{fiber} about $\bar{I}_4^*$ (Pandolfi and Vasta, 2012):

$$\Psi_{\text{fiber}}^{\text{V}} \approx \Psi_{\text{fiber}}(\bar{I}_4^*) + \frac{1}{2}\left.\frac{\partial^2 \Psi_{\text{fiber}}}{\partial \bar{I}_4^2}\right|_{\bar{I}_4=\bar{I}_4^*} \langle (\bar{I}_4 - \bar{I}_4^*)^2 \rangle = \overline{\Psi}_{\text{fiber}}^*\left(1 + K^*\sigma_{I_4}^2\right) + \Psi_{\text{fiber}}^0,$$

where, according to (5), we denote

$$K^* = K(\bar{I}_4^*)$$

and

$$\sigma_{I_4}^2 = \overline{\mathbf{C}} : \mathbb{H} : \overline{\mathbf{C}} - (\mathbf{H} : \overline{\mathbf{C}})^2, \quad \mathbb{H} = \langle \mathbf{A} \otimes \mathbf{A} \rangle.$$

The components of the forth order tensor $\mathbb{H}$ can be found in Vasta et al. (2013). The second Piola–Kirchhoff stress is obtained analytically as

$$\overline{\mathbf{S}}_{\text{fiber}}^{\text{V}} = \left(\alpha^{\text{M}} + \sigma_{I_4}^2\alpha^{\text{V}}\right)\mathbf{H} + \beta\mathbb{H} : \overline{\mathbf{C}}. \tag{14}$$

where

$$\alpha^{\text{M}} = \overline{\Psi}_{\text{fiber}}^* \sum_{j=0}^{3} a_j^{\text{M}} \bar{I}_4^{*j}, \quad \alpha^{\text{V}} = \overline{\Psi}_{\text{fiber}}^* \sum_{j=0}^{3} a_j^{\text{V}} \bar{I}_4^{*j}, \quad \beta = \overline{\Psi}_{\text{fiber}}^* \sum_{j=0}^{2} b_j \bar{I}_4^{*j}.$$

The tangent stiffness reads as

$$\overline{\mathbb{C}}^{\mathrm{V}}_{\mathrm{fiber}} = 4J^{-4/3}\left[\left(\gamma^{\mathrm{M}} + \sigma^2_{I_4}\gamma^{\mathrm{V}}\right)\mathbf{H}\otimes\mathbf{H} + \delta\mathbf{H}\otimes\mathbb{H} : \overline{\mathbf{C}} + 2\beta\mathbb{H}\right], \tag{15}$$

where

$$\gamma^{\mathrm{M}} = \overline{\Psi}^{*}_{\mathrm{fiber}}\sum_{j=0}^{4} c^{\mathrm{M}}_j \bar{I}^{*j}_4, \quad \gamma^{\mathrm{V}} = \overline{\Psi}^{*}_{\mathrm{fiber}}\sum_{j=0}^{4} c^{\mathrm{V}}_j \bar{I}^{*j}_4, \quad \delta = \overline{\Psi}^{*}_{\mathrm{fiber}}\sum_{j=0}^{3} d_j \bar{I}^{*j}_4.$$

The coefficients $a^{\mathrm{M}}_j, a^{\mathrm{V}}_j, b_j, c^{\mathrm{M}}_j, c^{\mathrm{V}}_j, d_j$ are listed in Table 1.

3. Planar distribution of fibers

A planar formulation may be obtained by specializing the distribution density $\bar{\rho}(\mathbf{a})$, see, e.g., Wang et al. (2012) and Vasta et al. (2013). We recall that, even for a planar distribution of the fibers, the derived structural tensor is a three-dimensional tensor, as well as the stress and stiffness tensors. We refer to a planar distribution lying on the plane normal to the direction $\mathbf{e}_1$ where we express the independence of the angle Φ by assuming

$$\bar{\rho}(\mathbf{a}) = \rho(\Theta), \tag{16}$$

with $\Theta \in [-\pi/2, \pi/2]$. The normalization condition (1) and the average definition (2) of a function $f(\mathbf{a}) = f(\Theta)$ in a planar setting become, respectively

$$\frac{1}{\pi}\int_{-\pi/2}^{\pi/2}\rho(\Theta)d\Theta = 1, \quad \langle f\rangle = \frac{1}{\pi}\int_{-\pi/2}^{\pi/2}\rho(\Theta)f(\Theta)\,d\Theta. \tag{17}$$

With no loss of generality, we account for a π-periodic distribution that depends only on the angle Θ and assume that the mean orientation of the fibers is in the direction $\mathbf{a}_0 = \mathbf{e}_3$. Thus, it is possible to derive the average structure tensor $\mathbf{H}^{\mathrm{pl}}$ for the planar distribution case (Vasta et al., 2013) as

$$\mathbf{H}^{\mathrm{pl}} = \begin{bmatrix} 0 & 0 & 0 \\ 0 & \kappa^{\mathrm{pl}} & 0 \\ 0 & 0 & 1-\kappa^{\mathrm{pl}} \end{bmatrix},$$

where

$$\kappa^{\mathrm{pl}} = \frac{1}{\pi}\int_{-\pi/2}^{\pi/2}\rho(\Theta)\sin^2\Theta\,d\Theta, \tag{18}$$

$$\hat{\kappa}^{\mathrm{pl}} = \frac{1}{\pi}\int_{-\pi/2}^{\pi/2}\rho(\Theta)\sin^4\Theta\,d\Theta \tag{19}$$

and the non-zero terms of the average fourth order tensor $\mathbb{H}^{\mathrm{pl}}$ are

$$H^{\mathrm{pl}}_{2222} = \hat{\kappa}^{\mathrm{pl}},$$
$$H^{\mathrm{pl}}_{3322} = H^{\mathrm{pl}}_{2233} = H^{\mathrm{pl}}_{3232} = H^{\mathrm{pl}}_{2323} = H^{\mathrm{pl}}_{3223} = H^{\mathrm{pl}}_{2332} = \kappa^{\mathrm{pl}} - \hat{\kappa}^{\mathrm{pl}},$$
$$H^{\mathrm{pl}}_{3333} = 1 - 2\kappa^{\mathrm{pl}} + \hat{\kappa}^{\mathrm{pl}}.$$

In order to perform numerical experiments described in the following, we select $\rho(\Theta)$ as the π-periodic normalized von Mises distribution centered at $\Theta = 0$ and given by

$$\rho(\Theta) = \frac{1}{\pi I^0}\exp\left(b\cos 2\Theta\right),$$

Table 1
Coefficients of the stress and tangent stiffness tensors in the second order or variance approximation.

Coeff.	$j=0$	$j=1$	$j=2$	$j=3$	$j=4$
a^{M}	$-4k_2$	$-8k_2^2$	$16k_2^2$	$-8k_2^2$	–
a^{V}	$-8k_2^3 - 12k_2^2$	$24k_2^3 + 12k_2^2$	$-24k_2^3$	$8k_2^3$	–
b	$8k_2^2 + 4k_2$	$-16k_2^2$	$8k_2^2$	–	–
c^{M}	–	$64k_2^3 + 96k_2^2$	$-192k_2^3 - 96k_2^2$	$1928k_2^3$	$-64k_2^3$
c^{V}	$32k_2^4 + 96k_2^3 + 24k_2^2$	$-128k_2^4 - 192k_2^3$	$192k_2^4 + 96k_2^3$	$-128k_2^4$	$328k_2^4$
d	$64k_2^3 - 96k_2^2$	$192k_2^3 + 96k_2^2$	$-192k_2^3$	$64k_2^3$	–

with

$$I^0 = \frac{1}{\pi}\int_{-\pi/2}^{\pi/2} \exp\left(b\cos 2\Theta\right) d\Theta.$$

The proposed choice is in line with several previous works addressing stochastic distributions of fibers in continuum media both for three- and two-dimensional material models (Gasser et al., 2006; Pandolfi and Vasta, 2012; Vasta et al., 2013). The von Mises distribution for several values of the concentration parameter b is visualized in Fig. 2(left). Fig. 2(right) shows the dependence of the coefficients κ^{pl} and $\widehat{\kappa}^{\mathrm{pl}}$ on the concentration parameter b. (see Fig. 3)

4. Fiber recruitment

The multiplicative decomposition of the deformation gradient fosters several advantages in the solution of nonlinear problems (Lubarda, 2004). The deformation gradient is assumed to split into an elastic part $\mathbf{F}_e$, related to the stress, and an inelastic part $\mathbf{F}_a$, that describes stress free kinematics:

$$\mathbf{F} = \mathbf{F}_e\mathbf{F}_a. \tag{20}$$

In keeping with the description provided in Hill et al. (2012), in the present study the inelastic part of the deformation gradient is assumed to provide a threshold for the onset of fiber recruitment. The threshold must be tuned against experimental measurements.

The approach considers three different configurations: (i) Ω_0, material (or stress free) configuration, where the lengths are denoted with L_0; (ii) Ω, spatial (or current) configuration were the lengths are denoted with l; (iii) Ω_a, intermediate configuration where the fibers are recruited and the lengths are denoted with L_a. The activation stretch λ_a, the elastic stretch λ_e, and the total stretch λ are defined as

$$\lambda_a = \frac{dL_a}{dL_0}, \quad \lambda_e = \frac{dl}{dL_a}, \quad \lambda = \frac{dl}{dL_0}. \tag{21}$$

In terms of stretches the multiplicative decomposition (20) becomes

$$\lambda = \lambda_e\,\lambda_a. \tag{22}$$

Note that the total stretch is related to the directional invariant $\bar{I}_4$

$$\bar{I}_4 \equiv \lambda^2 = \mathbf{A} : \overline{\mathbf{C}}. \tag{23}$$

As customary within the multiplicative decomposition approach, the mechanical response is shifted to the configuration Ω_a (Hill et al., 2012).

In the following, we will make use of the Leibniz's integral rule for functional differentiation under the integral sign, that we recall here for the sake of completeness. For a function $f(x,\omega)$ continuous with its partial derivative $\partial f(x,\omega)/\partial\omega$, it holds:

$$\frac{\partial}{\partial\omega}\int_{u(\omega)}^{v(\omega)} f(x,\omega)dx = \int_{u(\omega)}^{v(\omega)} \frac{\partial f(x,\omega)}{\partial\omega}dx + f(v(\omega),\omega)\frac{\partial v(\omega)}{\partial\omega} - f(u(\omega),\omega)\frac{\partial u(\omega)}{\partial\omega}. \tag{24}$$

By restricting our investigation to a planar distribution of the fiber orientation, we begin by considering an invariant based, integral formulation of the recruitment strain energy density $\Psi^{\mathrm{R}}_{\mathrm{fiber}}$ in the form

$$\Psi^{\mathrm{R}}_{\mathrm{fiber}} = \frac{1}{2\pi}\int_{-\pi/2}^{\pi/2} A(\bar{I}_4)\rho(\Theta)\,d\Theta,$$

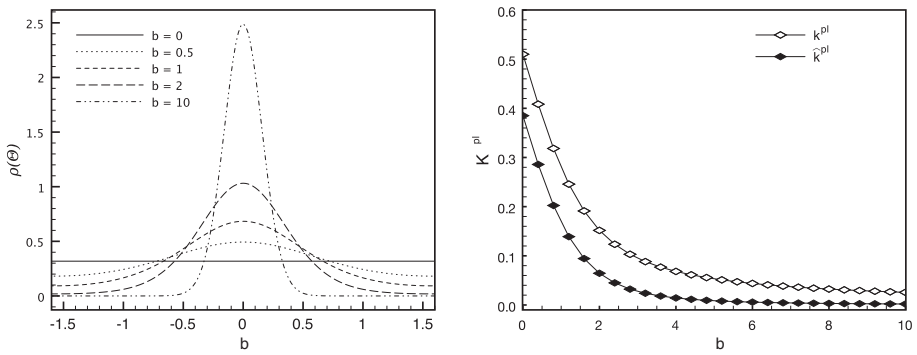

Fig. 2. (Left) Normalized von Mises distribution for five values of the concentration parameter b. (Right) Dependence of the concentration parameters κ^{pl}, Eq. (18), and $\widehat{\kappa}^{\mathrm{pl}}$, Eq. (19), on the concentration parameter b.

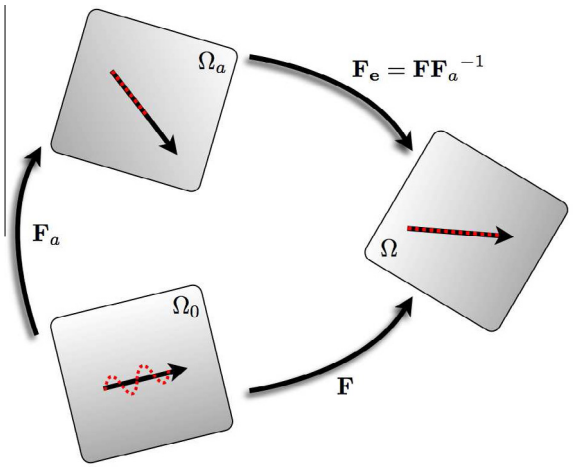

Fig. 3. Schematic representation of the multiplicative decomposition of the deformation deformation gradient tensor (20) in presence of fibers recruitment.

where $A(\bar{I}_4)$ is a recruitment function dependent on the normalized probability distribution function (PDF) of fiber recruitment $d_1(\lambda_a)$:

$$A(\bar{I}_4) = \int_1^{\sqrt{\bar{I}_4}} d_1(\lambda_a)\Psi_{\text{fiber}}(\bar{I}_4;\lambda_a)\,d\lambda_a, \quad \int_1^{\infty} d_1(\lambda_a)\,d\lambda_a = 1. \tag{25}$$

The functional form of Eq. (25) is taken from Hill et al. (2012). The amount $d_1(\lambda_a)\,d\lambda_a$ represents the portion of fibers lying in direction Θ (the angle Θ is tacitly included in $\bar{I}_4$) that uncrimps at the stretch λ_a, and $d_1(\lambda_a)\Psi_{\text{fiber}}(\bar{I}_4;\lambda_a)\,d\lambda_a$ is the corresponding contribution to the strain energy. It is natural to assume that recruitment occurs only when the stretch λ_a exceeds an activation threshold value λ_a^T in extension, i. e., for $\Delta\lambda = \lambda_a - \lambda_a^T \geqslant 0$, according to

$$d_1(\lambda_a) = \begin{cases} 0 & \text{if } \Delta\lambda < 0 \\ \frac{\Delta\lambda^{\alpha-1}e^{-\Delta\lambda/\beta}}{\beta^\alpha\Gamma(\alpha)}, \quad (\alpha>0,\beta>0) & \text{if } \Delta\lambda \geqslant 0, \end{cases} \tag{26}$$

where $\Gamma(.)$ is the Gamma function. For the two sets of parameters listed in Table 2, Fig. 4 visualizes the recruitment activation function $d_1(\lambda_a)$ versus the activation stretch λ_a and the cumulated function $D_1(\lambda_a)$, Eq. $(25)_2$, versus the total stretch λ, respectively.

Since our goal is a second order approximation of the recruitment strain energy density in the spirit of Pandolfi and Vasta (2012), we need to consider the Taylor expansion up to quadratic terms of $A(\bar{I}_4)$ about the average pseudo-invariant $\bar{I}_4^*$:

$$A(\bar{I}_4) \simeq A^* + \frac{\partial A^*}{\partial \bar{I}_4}\Delta I + \frac{1}{2}\frac{\partial^2 A^*}{\partial \bar{I}_4 \partial \bar{I}_4}\Delta I^2, \tag{27}$$

where $\Delta I = \bar{I}_4 - \bar{I}_4^*$ and the symbol * means evaluation of the term in $\bar{I}_4^*$. The coefficients of (27) are obtained by using Eq. (24) and the condition $\Psi_{\text{fiber}}(1;\lambda_a) = 0$:

$$A^* = \int_1^{\sqrt{\bar{I}_4^*}} d_1(\lambda_a)\Psi_{\text{fiber}}(\bar{I}_4^*;\lambda_a)\,d\lambda_a,$$

$$\frac{\partial A^*}{\partial \bar{I}_4} = \int_1^{\sqrt{\bar{I}_4^*}} d_1(\lambda_a)\Psi'_{\text{fiber}}(\bar{I}_4^*;\lambda_a)\,d\lambda_a, \tag{28}$$

$$\frac{\partial^2 A^*}{\partial \bar{I}_4 \partial \bar{I}_4} = \int_1^{\sqrt{\bar{I}_4^*}} d_1(\lambda_a)\Psi''_{\text{fiber}}(\bar{I}_4^*;\lambda_a)\,d\lambda_a + d_1\left(\sqrt{\bar{I}_4^*}\right)\frac{\Psi'_{\text{fiber}}(1;\lambda_a)}{2\sqrt{\bar{I}_4^*}}. \tag{29}$$

Table 2
Material parameters for the second order approximation fiber recruitment model used in the numerical simulation of the uniaxial tests documented in Hill et al. (2012). The 'Optimal' set is calibrated on experimental results; the 'Abrupt' set is selected to model an instantaneous activation of all the fibers.

Case	K [MPa]	μ_1 [MPa]	k_1 [MPa]	k_2 –	b –	λ_a^T –	α –	β –
Optimal	0	0.11	3.15	0.02	10	1.35	4.4	0.065
Abrupt	0	0.11	0.015	0.55	10	1	1.4	0.015

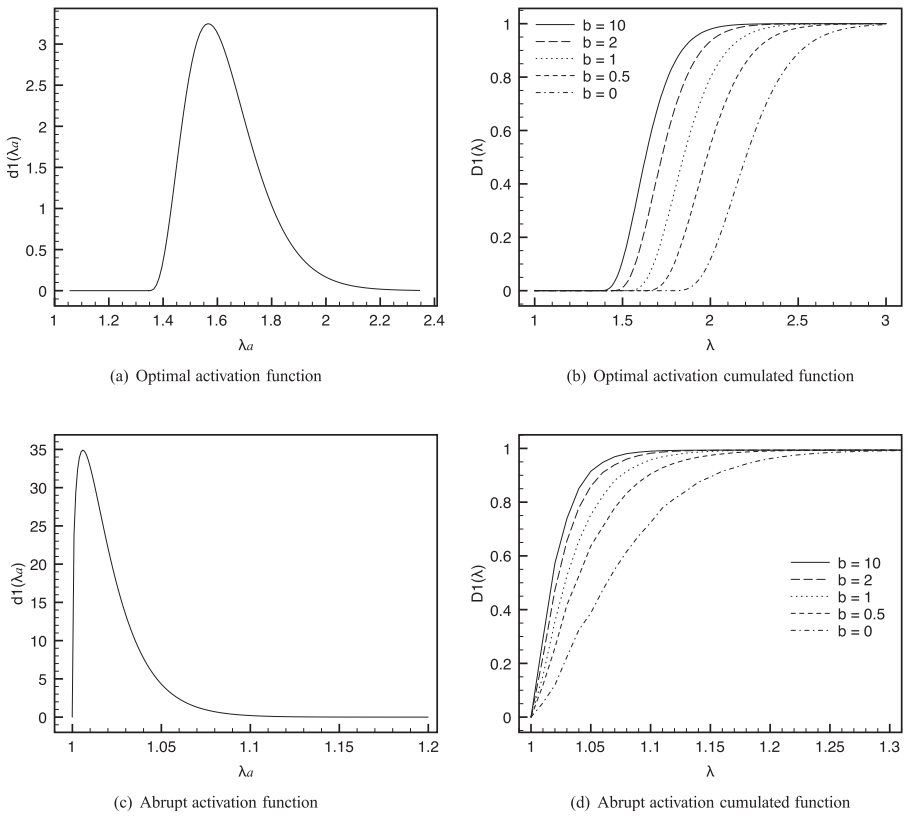

(a) Optimal activation function

(b) Optimal activation cumulated function

(c) Abrupt activation function

(d) Abrupt activation cumulated function

Fig. 4. (a,c): Activation recruitment function $d_1(\lambda_a)$, Eq. (26), versus the activation stretch λ_a (left). (b,d): Cumulated activation function $D_1(\lambda_a)$, Eq. $(25)_2$, versus the total stretch λ, for five different values of the concentration parameter b. (a,b): Optimal or delayed activation. (c,d): Abrupt or instantaneous activation of all the fibers. Material parameters are listed in Table 2.

In (28) and (29) we set:

$$\Psi'_{\text{fiber}}(\bar{I}_4^*;\lambda_a)=\left.\frac{\partial\Psi_{\text{fiber}}(\bar{I}_4;\lambda_a)}{\partial\bar{I}_4}\right|_{\bar{I}_4=\bar{I}_4^*},\quad \Psi''_{\text{fiber}}(\bar{I}_4^*;\lambda_a)=\left.\frac{\partial^2\Psi_{\text{fiber}}(\bar{I}_4;\lambda_a)}{\partial\bar{I}_4\partial\bar{I}_4}\right|_{\bar{I}_4=\bar{I}_4^*}.$$

The second order approximation of the recruitment energy density (25) follows from $(17)_2$:

$$\Psi^{\text{R}}_{\text{fiber}}\approx A^*+\frac{1}{2}\frac{\partial^2 A^*}{\partial\bar{I}_4\partial\bar{I}_4}\sigma^2_{I_4}.$$

In order to obtain the explicit expression of the stress and tangent stiffness tensors, we need to specify the functional form of $\Psi_{\text{fiber}}(\bar{I}_4;\lambda_a)$. By defining the elastic pseudo-invariant $\bar{I}_4^e$ as

$$\bar{I}_4^e=\frac{\bar{I}_4}{\lambda_a^2},$$

we introduce a slight modification of the exponential fiber orientation energy density (3) as

$$\Psi_{\text{fiber}}(\bar{I}_4;\lambda_a)=\overline{\Psi}_{\text{fiber}}(\bar{I}_4^e)+\Psi^0_{\text{fiber}}=\frac{k_1}{2k_2}\exp\left[k_2(\bar{I}_4^e-1)^2\right]-\frac{k_1}{2k_2}. \tag{30}$$

The exponential form (30) satisfies the normalization condition $\Psi_{\text{fiber}}(1;\lambda_a)=0$ and additionally possesses the useful property $\Psi'_{\text{fiber}}(1;\lambda_a)=0$. The second order energy recruitment integral acquires an explicit form

$$\Psi^{\text{R}}_{\text{fiber}}=\int_1^{\sqrt{\bar{I}_4}} d_1(\lambda_a)\,\overline{\Psi}^{e*}_{\text{fiber}}\left(1+\frac{K^{e*}}{\lambda_a^4}\sigma^2_{I_4}\right)d\lambda_a, \tag{31}$$

where we set

$$\overline{\Psi}^{e*}_{\text{fiber}} = \overline{\Psi}_{\text{fiber}}\left(\bar{I}^{e*}_4;\lambda_a\right), \quad K^{e*} = K(\bar{I}^{e*}_4), \quad \bar{I}^{e*}_4 = \frac{\bar{I}^{*}_4}{\lambda_a^2}.$$

In contrast with other recruitment models proposed in the literature (Hill et al., 2012), the strain energy density (31) leads to the explicit expression of the second Piola–Kirchhoff stress, characterized by the presence of the variance $\sigma^2_{I_4}$ in additive form

$$\overline{\mathbf{S}}^{\text{R}}_{\text{fiber}} = \left(\alpha^{\text{M}}_{\text{R}} + \sigma^2_{I_4}\alpha^{\text{V}}_{\text{R}}\right)\mathbf{H} + \beta_{\text{R}}\,\mathbb{H} : \overline{\mathbf{C}}, \tag{32}$$

where the coefficients are

$$\begin{aligned}
\alpha^{\text{M}}_{\text{R}} &= \int_1^{\sqrt{\bar{I}^{*}_4}} d_1(\lambda_a)\,\alpha^{\text{M}}_a\,d\lambda_a, \quad \alpha^{\text{M}}_a = \overline{\Psi}^{e*}_{\text{fiber}}\sum_{j=0}^{3}\frac{a^{\text{M}}_j}{\lambda_a^2}\,\bar{I}^{e*j}_4,\\
\alpha^{\text{V}}_{\text{R}} &= \int_1^{\sqrt{\bar{I}^{*}_4}} d_1(\lambda_a)\,\alpha^{\text{V}}_a\,d\lambda_a + D, \quad \alpha^{\text{V}}_a = \overline{\Psi}^{e*}_{\text{fiber}}\sum_{j=0}^{3}\frac{a^{\text{V}}_j}{\lambda_a^6}\,\bar{I}^{e*j}_4,\\
\beta_{\text{R}} &= \int_1^{\sqrt{\bar{I}^{*}_4}} d_1(\lambda_a)\,\beta_a\,d\lambda_a, \quad \beta_a = \overline{\Psi}^{e*}_{\text{fiber}}\sum_{j=0}^{2}\frac{b_j}{\lambda_a^4}\,\bar{I}^{e*j}_4.
\end{aligned} \tag{33}$$

Notably, the two stresses (14) and (32) have the same functional form, and the recruitment activity in (32) is fully accounted for by the three coefficients $\alpha^{\text{M}}_{\text{R}}, \alpha^{\text{V}}_{\text{R}}$ and β_{R}. The variance coefficient $\alpha^{\text{V}}_{\text{R}}$ shows a more complex structure with respect to α^{V}, because the use of (24) in the Taylor series approximation produces the additional term D, whose expression is reported in Appendix.

The recruitment tangent stiffness shows an analytical structure formally identical to (15)

$$\overline{\mathbb{C}}^{\text{R}}_{\text{fiber}} = 4J^{-4/3}\left[\left(\gamma^{\text{M}}_{\text{R}} + \sigma^2_{I_4}\gamma^{\text{V}}_{\text{R}}\right)\mathbf{H}\otimes\mathbf{H} + \delta_{\text{R}}\mathbf{H}\otimes\mathbb{H} : \overline{\mathbf{C}} + 2\beta_{\text{R}}\mathbb{H}\right)\Big]$$

where

$$\gamma^{\text{M}}_{\text{R}} = \frac{1}{2}\frac{\partial\alpha^{\text{M}}_{\text{R}}}{\partial\bar{I}^{*}_4} - \alpha^{\text{V}}_{\text{R}}\bar{I}^{*}_4, \quad \gamma^{\text{V}}_{\text{R}} = \frac{1}{2}\frac{\partial\alpha^{\text{V}}_{\text{R}}}{\partial\bar{I}^{*}_4}, \quad \delta_{\text{R}} = \frac{1}{2}\frac{\partial\beta_{\text{R}}}{\partial\bar{I}^{*}_4} + \alpha^{\text{V}}_{\text{R}}$$

and

$$\begin{aligned}
\frac{\partial\alpha^{\text{M}}_{\text{R}}}{\partial\bar{I}^{*}_4} &= \int_1^{\sqrt{\bar{I}^{*}_4}} d_1(\lambda_a)\,\frac{\partial\alpha^{\text{M}}_a(\bar{I}^{*}_4;\lambda_a)}{\partial\bar{I}^{*}_4}\,d\lambda_a - d_1\left(\sqrt{\bar{I}^{*}_4}\right)\frac{2k_1}{\bar{I}^{*}_4},\\
\frac{\partial\alpha^{\text{V}}_{\text{R}}}{\partial\bar{I}^{*}_4} &= \int_1^{\sqrt{\bar{I}^{*}_4}} d_1(\lambda_a)\,\frac{\partial\alpha^{\text{V}}_a(\bar{I}^{*}_4;\lambda_a)}{\partial\bar{I}^{*}_4}\,d\lambda_a + \frac{\partial D}{\partial\bar{I}^{*}_4},\\
\frac{\partial\beta_{\text{R}}}{\partial\bar{I}^{*}_4} &= \int_1^{\sqrt{\bar{I}^{*}_4}} d_1(\lambda_a)\,\frac{\partial\beta_a(\bar{I}^{*}_4;\lambda_a)}{\partial\bar{I}^{*}_4}\,d\lambda_a + d_1\left(\sqrt{\bar{I}^{*}_4}\right)\frac{2k_1}{\bar{I}^{*\,2}_4}.
\end{aligned} \tag{34}$$

The expression of the coefficient $\partial D/\partial\bar{I}^{*}_4$ can be found in Appendix.

5. Numerical tests

The second order fiber recruitment material model has been validated against uniaxial experimental data on carotid arteries documented in Hill et al. (2012). For the sake of comparison, we selected the expressions of $\Psi_{\text{volumetric}}(J)$ and $\Psi_{\text{matrix}}(\overline{\mathbf{C}})$ according to the choice described in Hill et al. (2012):

$$\Psi_{\text{volumetric}}(J) = 0, \quad \Psi_{\text{matrix}}(\overline{\mathbf{C}}) = \mu_1(\bar{I}_2 - 3),$$

although this choice implies a kinematic drawback pointed out in the recent literature (Murphy, 2013; Destrade et al., 2013; Pucci and Saccomandi, 2014). Through preliminary calculations on the average experimental results, we calibrated an optimal set of material parameters to be used in the subsequent calculations. The material parameters are listed in Table 2.

Fig. 5 compares uniaxial numerical results with the average experimental curve. Fig. 5(a) and (c) visualize numerical stress–strain curves in terms of first and second order approximation, respectively, for different values of the concentration parameter b and compare them with the average data reported in Hill et al. (2012). The optimal fitting is recovered for $b = 10$ in both approximations, reflecting the fact that the carotid samples tested in Hill et al. (2012) are characterized by a strong fibers alignment.

Note that the material response is affected by the value of the concentration parameter b. The dependence of the material response on b is further demonstrated in Fig. 5(b) and (d), where the Cauchy stress is plotted versus the parameter b for the first and second order approximation, respectively, considering four different values of the stretch in direction $\mathbf{a}_0 = \mathbf{e}_3$. For

the smallest value of the stretch considered, $\lambda = 1.3$, the recruitment process is not activated. In that case, in fact, $\lambda < \lambda_a^T$ and the resulting stress is constant for all b in both first and second order models. For all the other curves instead $\lambda > \lambda_a^T$, and, for the second order approximation, at small values of b a local maximum in the stress response appears. The peak is observed at the onset of the recruitment process for non negligible values of the k and $\dot{k}$ parameters. Contrariwise, the peak is not observed in the response of the mean approximation, confirming that the strong nonlinearity hidden in the recruitment model cannot be captured by a first order approximation. Interestingly, the presence of a local peak in the stress explains the interlacing of the stress–strain curves visible in Fig. 5(c) for the second order approximation, observed for small values of b and relatively high stretches. Curves interlacing is not observed for the first order approximation, see Fig. 5(a).

The influence of the recruitment process on the mechanical response is visualized in Fig. 6. The plot shows the numerical uniaxial curves obtained with a set of material parameters selected in order to model the experimental data in Hill et al. (2012) assuming the instantaneous activation of the recruitment process, see the set 'Abrupt' listed in Table 2. The response is compared with the one of the hyperelastic model with no recruitment described in Vasta et al. (2013). In general, when the recruitment process is not considered, the mechanical response is stiffer. Interesting, for any value of b, the uniaxial curves show a similar increasing trend for increasing λ, with the maximum discrepancy between abrupt recruitment and no recruitment at $b = 0$, see Fig. 6(a). Conversely, the stress versus concentration parameter curves pinpoint the strong nonlinearity introduced by the recruitment process, see Fig. 6(b). In the latter plot, the maximum discrepancy in the response is observed in correspondence of the maximum stretch, i.e., $\lambda = 0.8$.

The relevance of the fiber recruitment process on the mechanical response is further demonstrated in Fig. 7, which shows uniaxial curves computed with the 'Optimal' material properties listed in Table 2 and considering the hyperelastic model with no recruitment described in Vasta et al. (2013). As expected, the response of the model with no recruitment is stiffer than the response of the model with recruitment: for the actual choice of material parameters, the resulting stresses are two order of magnitude larger, cf. Fig. 5(c) and (d). Additionally, another calculation, based on the hyperelastic model with no recruitment described in Vasta et al. (2013) and adopting an alternative set of material parameters able to fit the experimental data in Hill et al. (2012), did not exhibit the localized peak in the stress response, diminishing sensibly the effects of the variance term.

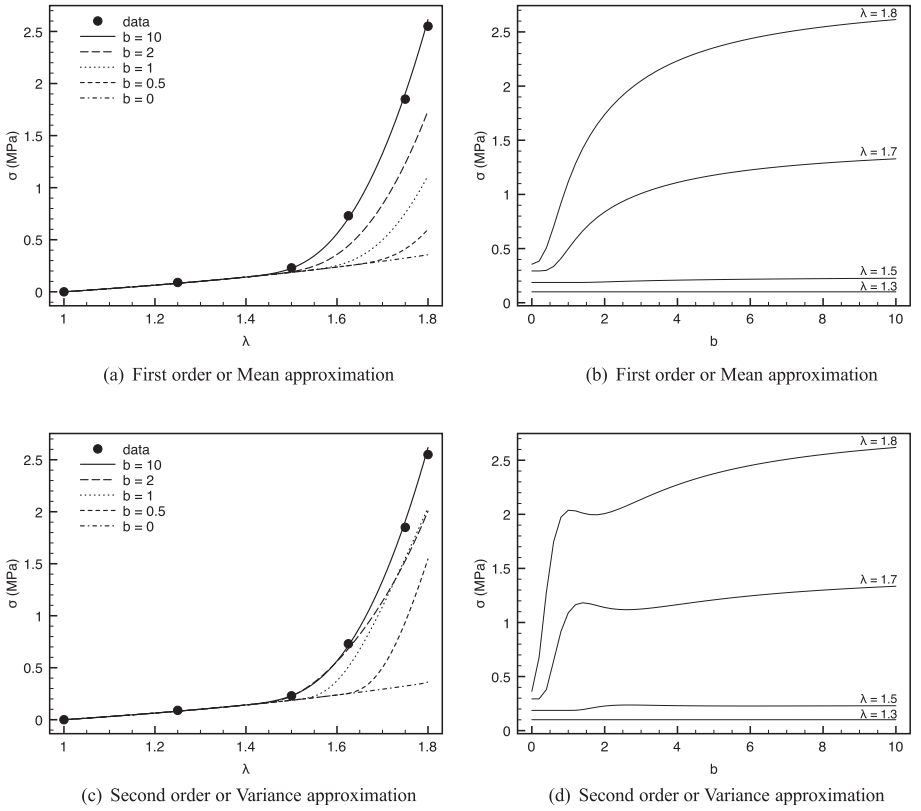

(a) First order or Mean approximation

(b) First order or Mean approximation

(c) Second order or Variance approximation

(d) Second order or Variance approximation

Fig. 5. Uniaxial tests in the direction $\mathbf{a}_0 = \mathbf{e}_3$. (a,b) Cauchy stress versus total stretch for (a) the first order or mean and (c) the second order or variance recruitment models. Black circles denote the average experimental curve on human carotid wall tissue documented in Hill et al. (2012). Curves refer to five values of the von Mises concentration parameter b, and the solid line, obtained for $b = 10$, shows the best agreement between model and experiment. (c,d) Cauchy stress versus the concentration parameter b for the (b) first and (d) second order recruitment model, for four different values of the final stretch. Material parameters (Optimal) are listed in Table 2.

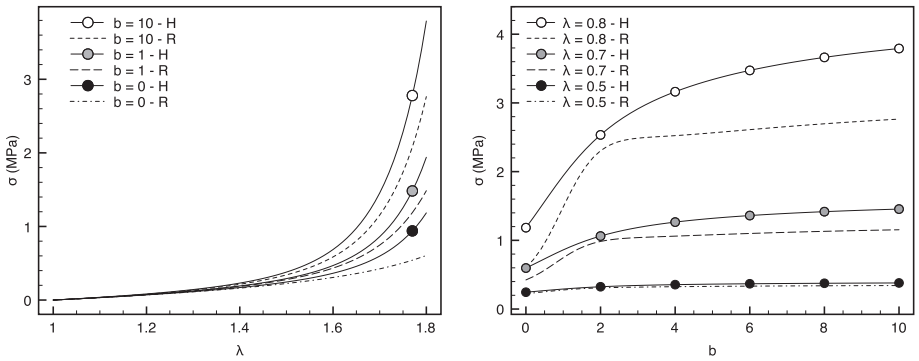

Fig. 6. Uniaxial test in the direction $\mathbf{a}_0 = \mathbf{e}_3$, comparison of the response with instantaneous recruitment and with no recruitment. Material parameters are listed in Table 2 (Abrupt). (Left) Cauchy stress with recruitment (R) and with no recruitment (H) versus the total stretch, for five values of the von Mises dispersion parameter b. (Right) Cauchy stress versus the dispersion parameter b for four different final stretches λ.

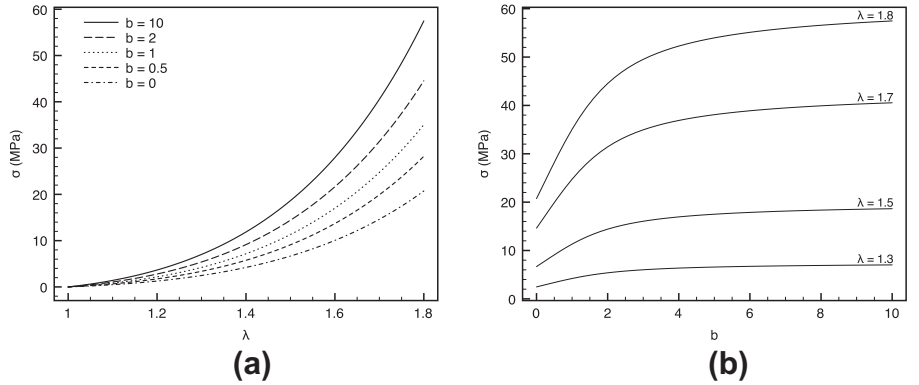

Fig. 7. Uniaxial tests in the direction $\mathbf{a}_0 = \mathbf{e}_3$ with no recruitment activation. (a) Cauchy stress versus total stretch for the second order, or variance, model. Curves refer to three values of the von Mises concentration parameter b. (b) Cauchy stress versus the concentration parameter b for four different values of the final stretch. Material parameters (Optimal) are listed in Table 2.

6. Conclusions

Fiber recruitment is a fundamental process in media with spatially dispersed fibers, among which we can classify fiber-reinforced biological tissues. In this contribution we depart from a well established hyperelastic model for fiber reinforced tissues (Gasser et al., 2006), in an extended form that includes the quadratic terms of a Taylor expansion about the average fourth pseudo-invariant $\bar{I}_4^*$ (Pandolfi and Vasta, 2012; Vasta et al., 2013), and, through the conventional multiplicative decomposition of the deformation gradient (Lubarda, 2004), we enrich the model by including a fiber recruitment function (Hill et al., 2012). The resulting recruitment strain energy density is a function of the average and of the variance of the directional pseudo-invariant $\bar{I}_4$. The Piola–Kirchhoff stress tensor and the tangent stiffness tensor are explicitly derived by differentiation of the strain energy density. In both stress and tangent stiffness tensors, the variance contribution can be pointed out analytically by in additive form.

The effect of the variance term is evident in the material response under uniaxial tests. In the case of a von Mises distribution of the fiber orientation, it is possible to observe that for an exponential expression of the fiber energy the mechanical response is very sensitive to the concentration parameter b. For the von Mises distribution, we calibrated an optimal set of material parameters able to fit the experimental data published in Hill et al. (2012): the average experimental uniaxial curve is well captured for $b = 10$. For the second order strain energy density in combination with the recruitment, we observe that the stress versus the concentration parameter b is characterized by a peak in correspondence of rather small values of b; the peak amplifies for relatively large stretches. The peak instead is not observed when the variance is not included in the strain energy density. For both strain energies we ascertained the high sensitivity of exponential material models on the dispersion parameters, and such behaviors pose a serious warning on the importance of calibrating the parameters against experimental data before numerical applications. A final comparison modeling the instantaneous activation of the recruitment process with respect to the hyperelastic material without recruitment activation results in similar stress trends, although the variance effect is more evident when the recruitment process is considered.

The general formulation proposed here can be regarded with particular interest in view of multidisciplinary and multiphysics applications. A first simple extension of the model will consider the presence of multiple set of fibers with a statistical distribution, in applications concerning the human cornea (Sanchez et al., submitted for publication) or the human skin (Ni Annaidh et al., 2012). In future studies, we foresee the combination of statistical recruitment and other biophysical phenomena, such as swelling in polymers (Baek and Pence, 2009), in particulate composites (Kanaun et al., 2008) or in realistic biomechanical tissue models (Gizzi et al., 2012) with microstructure (Ogden and Saccomandi, 2007; Ruiz-Baier et al., 2013). This will call for further generalizations of the theoretical framework here presented in order to account for such complex phenomena.

Appendix A

Functional coefficients for the Piola–Kirchhoff stress tensor Eq. (32):

$$
\begin{aligned}
&D = \frac{1}{2} k_1 \bar{I}_4^{*\,-5/2} d_1\left(\sqrt{\bar{I}_4^*}\right)\\
&\frac{\partial D}{\partial \bar{I}_4^*} = \left[\frac{k_1}{4\beta}\frac{5\beta + (\beta\alpha - 6\beta + 1)\sqrt{\bar{I}_4^*} - \bar{I}_4^*}{\bar{I}_4^{*\,7/2}\left(\sqrt{\bar{I}_4^*} - 1\right)}\right] d_1\left(\sqrt{\bar{I}_4^*}\right).
\end{aligned}
\tag{35}
$$

$$
\begin{aligned}
&\alpha_{\mathrm{R}}^{\mathrm{M}} = 4\int_1^{\sqrt{\bar{I}_4^*}} \frac{d_1(\lambda_a)}{\lambda_a^4}\overline{\Psi}^*\left(\mathcal{M}^*\lambda_a^2 - \bar{I}_4^* K^*\right) d\lambda_a\\
&\alpha_{\mathrm{R}}^{\mathrm{V}} = 4\int_1^{\sqrt{\bar{I}_4^*}} \frac{d_1(\lambda_a)}{\lambda_a^6}\overline{\Psi}^*(2k_2 + K^*)\mathcal{M}^* d\lambda_a + D\left(\bar{I}_4^*\right)\\
&\beta_{\mathrm{R}} = 4\int_1^{\sqrt{\bar{I}_4^*}} \frac{d_1(\lambda_a)}{\lambda_a^4}\overline{\Psi}^* K^* d\lambda_a,\\
&\frac{\partial\sqrt{\bar{I}_4^*}}{\partial\overline{\mathbf{C}}} = \frac{1}{2\sqrt{\bar{I}_4^*}}\mathbf{H}, \quad \frac{\partial\sigma_{\bar{I}_4}^2}{\partial\overline{\mathbf{C}}} = 2\mathbb{H} : \overline{\mathbf{C}} - 2\bar{I}_4^*\mathbf{H},\\
&\frac{\partial\Psi'^*}{\partial\overline{\mathbf{C}}} = \frac{1}{\lambda_a^2}\overline{\Psi}^{*\prime}\mathbf{H}, \quad \frac{\partial(K^*\overline{\Psi}^*)}{\partial\overline{\mathbf{C}}} = \frac{1}{\lambda_a^2}\left[K^{*\prime}\overline{\Psi}^* + K^*\overline{\Psi}^{*\prime}\right]\mathbf{H}.
\end{aligned}
$$

References

Alastrué, V., Martinez, M. A., Menzel, A., & Doblaré, M. (2006). On the use of non-linear transformations for the evaluation of anisotropic rotationally symmetric directional integrals. Application to the stress analysis in fibred soft tissues. *International Journal for Numerical Methods in Engineering, 128*, 150–160.

Baek, S., & Pence, T. J. (2009). On swelling induced degradation of fiber reinforced polymers. *International Journal of Engineering Science, 117*, 1100–1109.

Cortes, D. H., Lake, S. P., Kadlowec, J. A., Soslowsky, L. J., & Elliott, D. M. (2010). Characterizing the mechanical contribution of fiber angular distribution in connective tissue: comparison of two modeling approaches. *Biomechanics and Modeling in Mechanobiology, 11*, 651–658.

Destrade, M., Saccomandi, G., & Sgura, I. (2009). Inhomogeneous shear of orthotropic incompressible non-linearly elastic solids: Singular solutions and biomechanical interpretation. *International Journal of Engineering Science, 47*, 1170–1181.

Destrade, M., Gilchrist, M. D., & Ogden, R. W. (2010). Third- and fourth- order elasticity of biological soft tissues. *Journal of the Acoustical Society of America, 127*, 2103–2106.

Destrade, M., Mac Donald, B., Murphy, J. G., & Saccomandi, G. (2013). At least three invariants are necessary to model the mechanical response of incompressible, transversely isotropic materials. *Computational Mechanics, 52*, 959–969.

Federico, S., & Gasser, T. C. (2010). Nonlinear elasticity of biological tissues with statistical fibre orientation. *Journal of the Royal Society Interface, 7*, 955–966.

Fereidoonnezhad, B., Naghdabadi, R., & Arghavani, J. (2013). A hyperelastic constitutive model for fiber-reinforced rubber-like materials. *International Journal of Engineering Science, 71*, 36–44.

Gasser, T. C., Ogden, R. W., & Holzapfel, G. A. (2006). Hyperelastic modelling of arterial layers with distributed collagen fibre orientations. *Journal of the Royal Society Interface, 3*, 15–35.

Gizzi, A., Cherubini, C., Pomella, N., Persichetti, P., Vasta, M., & Filippi, S. (2012). Computational modeling and stress analysis of columellar biomechanics. *Journal of the Mechanical Behavior of Biomedical Materials, 15*, 46–58.

Hill, M. R., Duan, X., Gibson, G. A., Watkins, S., & Robertson, A. M. (2012). A theoretical and non-destructive experimental approach for direct inclusion of measured collagen orientation and recruitment into mechanical models of the artery wall. *Journal of Biomechanics, 45*, 762–771.

Holzapfel, G. A., Gasser, T. C., & Ogden, R. W. (2000). A new constitutive framework for arterial wall mechanics and a comparative study of material models. *Journal of Elasticity, 61*, 1–48.

Kanaun, S., Levin, V., & Pervago, E. (2008). Acoustical and optical branches of wave propagation in random particulate composites. *International Journal of Engineering Science, 46*, 352–373.

Kroon, M., & Holzapfel, G. A. (2008). A new constitutive model for multi-layered collagenous tissues. *Journal of Biomechanics, 41*, 2766–2771.

Landau, L. D., & Lifshitz, E. M. (1986). *Theory of elasticity*. Oxford: Butterworth-Heineman.

Lanir, Y. (1979). A structural theory for the homogeneous biaxial stress–strain relationship in flat collagenous tissues. *Journal of Biomechanics, 12*, 423–436.

Lanir, Y. (1983). Constitutive equations for fibrous connective tissues. *Journal of Biomechanics, 16*, 1–12.

Li, D., & Robertson, A. M. (2009). A structural multi-mechanism constitutive equation for cerebral arterial tissue. *International Journal of Solids and Structures, 46*, 2920–2928.
Lubarda, V. A. (2004). Constitutive theories based on the multiplicative decomposition of deformation gradient: Thermoelasticity, elastoplasticity, and biomechanics. *Applied Mechanics Review, 57*, 95–108.
Megens, R. T. A., Reitsma, S., Schiffers, P. H. M., Hilgers, R. H. P., De Mey, J. G. R., Slaaf, D. W., et al (2007). Two-photon microscopy of vital murine elastic and muscular arteries. *Journal of Vascular Research, 44*, 87–98.
Merodio, J., & Ogden, R. W. (2005). Tensile instabilities and ellipticity in fiber-reinforced compressible non-linearly elastic solids. *International Journal of Engineering Science, 43*, 697–706.
Murphy, J. G. (2013). Transversely isotropic biological, soft tissue must be modelled using both anisotropic invariants. *European Journal of Mechanics-A/Solids, 42*, 90–96.
Ni Annaidh, A., Bruyere, K., Destrade, M., Gilchrist, M. D., Maurini, C., Ottenio, M., et al (2012). Automated estimation of collagen fibre dispersion in the dermis and its contribution to the anisotropic behaviour of skin. *Annals of Biomedical Engineering, 40*, 1666–1678.
Ogden, R. W., & Saccomandi, G. (2007). Introducing mesoscopic information into constitutive equations for arterial walls. *Biomechanics and Modeling in Mechanobiology, 6*, 333–344.
Pandolfi, A., & Vasta, M. (2012). Fiber distributed hyperelastic modeling of biological tissues. *Mechanics of Materials, 44*, 151–162.
Pinsky, P. M., van der Heide, D., & Chernyak, D. (2005). Computational modeling of mechanical anisotropy in the cornea and sclera. *Journal of Cataract & Refractive Surgery, 31*, 136–145.
Pucci, E., & Saccomandi, G. (2014). On the use of universal relations in the modeling of transversely isotropic materials. *International Journal of Solids and Structures, 51*, 377–380.
Raghupathy, R., & Barocas, V. H. (2009). A closed-form structural model of planar fibrous tissue mechanics. *Journal of Biomechanics, 42*, 1424–1428.
Roach, M. R., & Burton, A. C. (1957). The reason for the shape of the distensibility curves of arteries. *Canadian Journal of Biochemistry and Physiology, 8*, 681–690.
Roy, S., Boss, C., Rezakhaniha, R., & Stergiopulos, N. (2010). Experimental characterization of the distribution of collagen fiber recruitment. *Journal of Biorheology, 2*, 84–93.
Ruiz-Baier, R., Gizzi, A., Rossi, S., Cherubini, C., Laadhari, A., Filippi, S., et al (2013). Mathematical modelling of active contraction in isolated cardiomyocytes. *Mathematical Medicine and Biology*. http://dx.doi.org/10.1093/imammb/dqt009.
Sacks, M. S. (2000). Biaxial mechanical evaluation of planar biological materials. *Journal of Elasticity, 8*, 681–690.
Sanchez, P., Moutsouris, K., Pandolfi, A. (submitted for publication). Biomechanical and optical behavior of human corneas undergoing refractive surgery. *Journal of Cataract and Refractive Surgery*.
Soldatos, K. P. (2009). Towards a new generation of 2D mathematical models in the mechanics of thin-walled fibre-reinforced structural components. *International Journal of Engineering Science, 11*, 1346–1356.
Vasta, M., Gizzi, A., Pandolfi, A. (in press). On three- and two-dimensional fiber distributed models of biological tissues. *Probabilistic Engineering Mechanics*.
Wang, Y., Son, S., Swartz, S. M., & Goulbourne, N. C. (2012). A mixed Von-Mises distribution for modelling biological tissues with two distributed fiber properties. *International Journal of Solids and Structures, 49*, 2914–2923.
Watton, P. N., Ventikos, Y., & Holzapfel, G. A. (2012). Modelling the mechanical response of elastin for arterial tissue. *Journal of Biomechanics, 42*, 1320–1325.
Wulandana, R., & Robertson, A. M. (2005). An inelastic multi-mechanism constitutive equation for cerebral arterial tissue. *Biomechanics and Modeling in Mechanobiology, 4*, 235–248.
Zoumi, A., Lu, X., Kassab, G. S., & Tromberg, B. J. (2004). Imaging coronary artery microstructure using second-harmonic and two-photon fluorescence microscopy. *Biophysical Journal, 87*, 2778–2786.